Title: Characterization of BRD4 during mammalian post-meiotic sperm development

Authors: Jessica M. Bryant[1,2,3], Greg Donahue[1], Xiaoshi Wang[4], Mirella Meyer-Ficca[5], Lacey J. Luense[1], Angela H. Weller[1], Marisa S. Bartolomei[1], Gerd A. Blobel[6], Ralph G. Meyer[5], Benjamin A. Garcia[4], and Shelley L. Berger[1,#]

[1]Epigenetics Program, Department of Cell and Developmental Biology, University of Pennsylvania Perelman School of Medicine, Philadelphia, Pennsylvania 19104, USA [2]Biomedical Graduate Studies, University of Pennsylvania [3]Current address: Institut Pasteur, Paris, France 75724 [4]Epigenetics Program, Department of Biochemistry and Biophysics, University of Pennsylvania Perelman School of Medicine, Philadelphia, Pennsylvania 19104, USA [5]Department of Animal Biology, School of Veterinary Medicine, University of Pennsylvania, Pennsylvania 19104, current address: Department of Animal, Dairy and Veterinary Sciences, School of Veterinary Medicine, College of Agriculture and Applied Sciences, Utah State University, Logan, Utah, 84322, USA [6]Division of Hematology, The Children's Hospital of Philadelphia, The Perelman School of Medicine at the University of Pennsylvania, Philadelphia, PA 19104, USA [#]Correspondence should be addressed to S.L.B. (e-mail: bergers@mail.med.upenn.edu)

Running title: Characterization of BRD4 in mammalian spermiogenesis

Materials and Methods word count: 2,011

Introduction, Results, and Discussion word count: 4,969

ABSTRACT

During spermiogenesis, the post-meiotic phase of mammalian spermatogenesis, transcription is progressively repressed as nuclei of haploid spermatids are compacted through a dramatic chromatin reorganization involving hyper-acetylation and replacement of most histones with protamines. Although BRDT functions in transcription and histone removal in spermatids, it is unknown whether other BET family proteins play a role. Immunofluorescence of spermatogenic cells revealed BRD4 in a ring around the nuclei of spermatids containing hyper-acetylated histones. The ring lies directly adjacent to the acroplaxome, the cytoskeletal base of the acrosome, previously linked to chromatin reorganization. The BRD4 ring does not form in acrosomal mutant mice. ChIP sequencing in spermatids revealed enrichment of BRD4 and acetylated histones at the promoters of active genes. BRD4 and BRDT show distinct and synergistic binding patterns, with a pronounced enrichment of BRD4 at spermatogenesis-specific genes. Direct association of BRD4 with acetylated H4 decreases in late spermatids as acetylated histones are removed from the condensing nucleus in a wave following the progressing acrosome. These data provide evidence for a prominent transcriptional role of BRD4 and suggest a possible removal mechanism for chromatin components from the genome via the progressing acrosome as transcription is repressed in response to chromatin condensation during spermiogenesis.

INTRODUCTION

Mammalian spermatogenesis has emerged as a focus of epigenetic study, as this conserved process requires vast changes in transcription and chromatin organization (1). Spermatogenesis, or the formation of the mature male gamete, takes place in the seminiferous tubules of the testes and begins with the stem-like spermatogonia. Diploid spermatogonia can differentiate into spermatocytes, which enter meiosis to produce four genetically unique haploid round spermatids (Fig. 1A). During the post-meiotic process of spermiogenesis, a spermatid differentiates into a motile spermatozoon by shedding most cytoplasm, forming a flagellum, and compacting the nucleus.

In mice, nuclear morphology changes dramatically during spermiogenesis: the nucleus is initially round (in round spermatids), then elongates (in elongating spermatids), and finally condenses into a small hook-like shape (in condensing/condensed spermatids) (Fig. 1A). This process is necessary for the formation of fertile sperm and involves chromatin compaction and consequent vast transcriptional repression (1). Nuclear compaction is accomplished via near-complete replacement of canonical histones, some with testes-specific histone variants; but most histones are initially replaced with transition proteins and then with protamines (2). Although several groups have shown that the small percentage of histones that remain associated with the genome in mature sperm are specifically post-translationally modified and enriched at developmentally important loci (3, 4) and gene regulatory sequences (5), recent studies have provided contrasting evidence that in mouse sperm, histone retention occurs preferentially in large gene-poor genomic regions (6-8). The mechanism by which almost all histones are removed and degraded has yet to be elucidated, but several important factors in this process have been discovered (9).

Chromatin reorganization during spermiogenesis begins concurrently with acrosome formation and histone hyper-acetylation. The acrosome is a cap-like, membrane-bound organelle derived from the Golgi apparatus that covers the apical part of the mature sperm nucleus. This organelle contains digestive enzymes that are released upon contact with the egg to facilitate fertilization. Acrosome biogenesis begins after meiosis is complete and is accomplished via fusion of fragments of the Golgi apparatus at the acroplaxome, or the cytoskeletal base of the forming acrosome (10). The acroplaxome consists of actin and keratin and anchors the acrosome to the adjacent nuclear membrane of the spermatid. Recently, several studies have linked acrosome biogenesis to the dramatic chromatin reorganization that takes place during spermiogenesis. Mouse mutants with defective acrosome formation produce abnormal, round-headed sperm that show defective nuclear compaction (11-15). Moreover, histone removal in human spermatids takes place adjacent to the acroplaxome as the acrosome progressively caps the nucleus (16). These studies suggest that acrosome biogenesis plays a role in sperm head shaping and nuclear compaction, but the mechanisms by which this may happen are unknown.

After meiosis is complete and acrosome formation has begun, histones become hyper-acetylated in the spermatid nucleus (17-19). Histone hyper-acetylation is believed to facilitate histone removal either through a direct loosening of the chromatin or via binding of bromodomain-containing proteins such as PA200, the activator of the “spermatoproteasome”, and BRDT, the testes-specific BET (Bromo- and Extra-Terminal domain) family protein (20-23). Like all BET family members, BRDT contains two bromodomains at its N-terminus and an extra-terminal (ET) domain at its C-terminus. Recently, BRDT has been shown to play a dual role during spermatogenesis (24). First, BRDT plays a transcriptional role, binding to

Molecular and Cellular Biology

Molecular and Cellular Biology

acetylated histones and P-TEFb at the promoters of meiotic and post-meiotic genes that are aberrantly repressed in its absence (25). In fact, *Brdt* knockout or treatment of male mice with JQ1 – a small-molecule inhibitor of BET family proteins – results in meiotic arrest and a significant decrease in fertility (25, 26). Second, BRDT may play a structural role in chromatin dynamics during spermiogenesis. Mice expressing BRDT lacking the first bromodomain show defects in fertility caused by abnormal nuclear compaction and chromatin organization during spermiogenesis (20, 27). However, it is unclear whether these later defects are again due to transcriptional de-regulation or rather to decreased binding of BRDT to hyper-acetylated histones.

It is also unclear whether other members of the BET family are integral to the process of spermatogenesis, as *Brd2* and *Brd4* null mouse mutants show embryonic lethality (28, 29). However, these genes are expressed during spermatogenesis at the mRNA and protein level (30). Interestingly, *Brd4* heterozygous null mice show defects in spermatogenesis, although this phenotype has not been well characterized (29). BRD4 has been shown to bind to the acetylated tails of histones H3 and H4 and is generally associated with active gene transcription (31). However, BRD4 also plays non-transcriptional roles such as tethering the human papilloma virus genome to host chromatin during mitosis (32).

In this study, we investigate BRD4 during spermiogenesis. We show that BRD4 is found in post-meiotic cells and investigate a novel BRD4 ring structure in spermatid nuclei that is closely associated with the acrosome. Moreover, we show with ChIP sequencing that BRD4 has an unanticipated prominent association with genes expressed in post-meiotic cells. Taken together, our results suggest an interesting mechanism for nuclear protein removal by linking BRD4 and transcription shutdown to acrosome formation during spermiogenesis.

RESULTS

BRD4 is expressed in meiotic cells and spermatids, but not in mature sperm

Although a transcriptional role of BRDT has been demonstrated during meiosis and spermiogenesis, it is unclear if other BET family proteins play a role in spermatogenesis (25). As mentioned above, *Brd4* heterozygous null male mice show spermatogenic defects, suggesting that BRD4 may play a role in spermatogenesis (28, 29). To investigate the expression pattern of BRD4 over the course of spermatogenesis, we analyzed protein levels in different cell types obtained by STA-PUT velocity sedimentation from mature mouse testes (33). With this method, we collected four cell populations (see Fig. 1A): 1) a mixture of meiotic cells (spermatocytes: Sc), 2) early post-meiotic spermatids (round spermatids: RSp), 3) later post-meiotic spermatids (elongating and condensing spermatids: E/CSp), and 4) a mixture of early and later spermatids (R/E/CSp). Mature sperm were isolated from the cauda epididymis of wild-type mice.

In addition to microscopic verification of purity via cellular and nuclear morphology [see (33) for our methods], we used western blot analysis of lysates from these cells to confirm relative purity. Although H4 protein is depleted in late spermatids (E/CSp), H4K5,8,12,16ac, but not H3K9ac, was relatively enriched in these elongating and condensing spermatids (Fig. 1B). This analysis also revealed the presence of the long isoform of BRD4 protein (indicated with an asterisk Fig. 1B) in meiotic cells ("Sc"), round spermatids ("RSp"), and elongating/condensing spermatids ("E/CSp"), but not in mature sperm ("Sperm"). A second smaller BRD4 isoform or degradation product was also detected in later spermatids (arrow in Fig. 1B, upper panel). The specificity of the BRD4 antibody for the long and shorter forms was confirmed by peptide competition (second panel, Fig. 1B). The canonical BRD4 short isoform

(~723aa) was not detected in any spermatogenic cells in this analysis. In addition to BRD4, BRDT and BRD2 are expressed over the course of spermatogenesis. While BRDT is expressed most highly in spermatocytes, BRD2 and BRD4 protein levels increase over the course of spermiogenesis.

BRD4 forms a ring around the nucleus of spermatids as histones become hyper-acetylated

To gain insight into a possible function for BRD4 during spermatogenesis, we determined its subcellular localization by performing indirect immunofluorescence (IF) on tissue sections from the testes of adult wild-type male mice. Using intact tissue allows for the identification of specific steps of spermatogenesis within the seminiferous tubules (34). Interestingly, we detected BRD4 in a distinct, complete ring around the nucleus beginning in approximately stage 7-8 spermatids (Sp) (Fig. 2A). The BRD4 ring is not present in spermatogonia or spermatocytes (Sc) (Fig. 2A) and appears concurrently with the post-meiotic hyper-acetylation of histones in the nucleus, not seen in spermatocytes (compare Sp to Sc in Fig. 2B). We confirmed that the apparently distinct "ring" is not associated with the entire nuclear periphery with pseudo-3D images created with z-stacked individual confocal images of early and late elongating spermatid nuclei (Movies A and B, resp.). We found the BRD4 structure closely changes shape along with the condensing nucleus of the spermatid: from round to oblong, always at the periphery of the DAPI-stained nucleus (Fig. 2A,B and Movies A,B). This ring structure is specific to BRD4, as IF analysis of a mixed population of spermatogenic cells showed BRD2 and BRDT in a diffuse nuclear staining pattern in spermatocytes and round spermatids (Fig. 2C,D).

BRD4 forms a ring within the nuclear envelope at the base of the acrosome

To further investigate the sub-cellular location of BRD4, we performed indirect IF for BRD4 and Lamin B1, a key component of the nuclear membrane. Co-detection of these proteins revealed that BRD4 is located at an important transitional region of the nuclear membrane in spermatids (Fig. 3A). More specifically, Lamin B1 and nuclear pores become polarized to the posterior end of the spermatid nuclear membrane, clearly distinct from the anterior end, which becomes closely covered by the acrosome (Fig. 3B, acrosome location indicated by an asterisk in Fig. 3A) (35-37). The acrosome is partly anchored to the nuclear envelope by a cytoskeletal plate called the acroplaxome, which forms a ring-like structure very similar to the BRD4 ring in the region where the Lamin B1-associated nuclear envelope meets the acrosome-associated nuclear envelope (Fig. 7D) (10). Therefore, we hypothesized that BRD4 may be associated with the acroplaxome.

To determine whether the BRD4 ring is linked to the acrosome/acroplaxome, we performed IF on spermatogenic cells, probing with fluorophore-conjugated peanut agglutinin (PNA) to detect the acrosome, or with phalloidin to detect actin in the acroplaxome (Fig. 3C and Movie C, respectively). Indeed, the BRD4 ring appears directly at the base of the acrosome during capping in late round spermatids (top panel) and persists in elongating (middle panel) and condensing spermatids (bottom panel) (Fig. 3C). Using a confocal microscope to create a pseudo-3D image, we discovered that the BRD4 ring lies just adjacent to the actin ring of the acroplaxome, but closer to the DAPI-stained nucleus (Movie C).

To provide additional evidence of the acrosome-associated BRD4 ring, we incubated spermatogenic cells with JQ1-biotin followed by fluorophore-conjugated streptavidin. JQ1 is a small molecule that binds to the bromodomains of all BET family proteins, which are expressed

Molecular and Cellular Biology

in the nucleus of multiple spermatogenic cell types [Fig. 2C,D and (30, 38, 39)]. Thus, JQ1-biotin shows a diffuse nuclear staining pattern in most spermatogenic cells types (Fig. 3D, top panel); however, this staining is not a random artifact of streptavidin binding (Fig. 3D, bottom panel). Importantly, in addition to a diffuse nuclear staining, JQ1-biotin is enriched in a ring structure that overlaps with the BRD4 ring in spermatids [late round (top panel) and elongating (bottom panel) spermatids in Fig. 3E]. Moreover, this JQ1-biotin enrichment is found at the base of the acrosome, providing additional evidence for the existence of the BRD4 ring (Fig. 3F).

Because the BRD4 ring and the acroplaxome are remarkably similar in shape and location, we hypothesized that acrosome formation is needed for BRD4 ring formation. To test this hypothesis, we analyzed *Hrb* (also known as *Agfg1*) null mice, which produce infertile sperm that lack acrosomes and have round, poorly compacted nuclei (11). In wild-type male mice, the acrosome is formed by the fusion at the acroplaxome of proacrosomic vesicles derived from the Golgi apparatus (Fig. 4A, top panels) (40). In $Hrb^{-/-}$ male mice, the proacrosomic vesicles begin to form in round spermatids, but they are unable to fuse properly to form a mature acrosome (Fig. 4A, bottom panels). $Hrb^{-/-}$ mice also show defects in nuclear elongation and compaction later in condensing spermatids when the acrosome is completely absent (Fig. 4A, bottom right panel).

To determine if acrosome development is required for BRD4 ring formation, we performed indirect IF on cryosectioned testes tissue from adult $Hrb^{+/-}$ (which have normal spermatogenesis) and $Hrb^{-/-}$ mice (11). Strikingly, the BRD4 ring does not form properly in $Hrb^{-/-}$ mice (Fig. 4B, right panel). A small amount of BRD4 can be seen around spermatid nuclei in $Hrb^{-/-}$ mice, but the conspicuous ring structure never develops and exists only in small

fragments, if at all, in late stage spermatids (Fig. 4B, right panel). Because the acroplaxome forms partially, although aberrantly, in *Hrb*$^{-/-}$ acrosomal mutant mice, it is possible that the BRD4 ring is able to form partially due to an association with certain components of the acroplaxome that may be able to assemble in *Hrb*$^{-/-}$ mice despite the lack of a functional acrosome (41).

BRD4 is enriched at the promoters of active genes in spermatids

It is possible that BRD4 is present diffusely throughout the nucleus in round spermatids, undetectable by IF until it is present in a higher concentration in the ring structure in very late round spermatids. To determine if BRD4 interacts with the genome in spermatids, we analyzed the genome-wide enrichment of BRD4 with chromatin immunoprecipitation followed by sequencing (ChIP-seq). We performed analysis in round spermatids to characterize BRD4 binding in the context of the distinct post-meiotic gene expression program, as a previous study has done for BRDT (25). We also determined the genome-wide localization of various other histone post-translational modifications (PTMs) to assess whether BRD4 shows a binding preference for any of these PTMs (all of which were normalized to input). All ChIP-seq data alignment information can be found in Table 1.

Upon initial examination of the ChIP-seq data, it is evident that BRD4 and H3 and H4 acetylation (H3/H4ac) are enriched in genic regions of the genome as opposed to an established heterochromatin PTM, H3K9me3, which is enriched in large intergenic regions (Fig. 5A). Indeed, bioinformatic analysis revealed that the majority of peaks of BRD4, H3ac, and H4ac are located within promoters [1 kilobasepair (kb) upstream of the transcriptional start site (TSS)] or genes (introns or exons), unlike H3K9me3, which is located primarily in intergenic regions (Fig.

232 5B). Upon closer examination, BRD4 is enriched at the TSS of active housekeeping genes such
233 as *Actb* and active spermatogenesis-specific genes such as *Tnp1* (Fig. 5C). Conversely, BRD4
234 is not found at repressed housekeeping genes such as *Myc* (Fig. 5C). BRD4 is not bound to all
235 active genes even though some, such as *Vps45*, may be enriched for H3 or H4 acetylation (Fig.
236 5C).

237 In addition, we did not observe significant differences in enrichment patterns among
238 acetylation at different H3 and H4 residues. In general, H3K9ac and H4K5, 8, 12, and 16ac
239 appear to be enriched surprisingly similarly at the TSS of active genes (Fig. 5A,C). Although
240 BRD4 is not present at the TSS of all active genes, heat map analysis revealed that levels of
241 BRD4, H3K9ac, and H4ac at gene promoters (green in Fig. 6A) show a strong correlation with
242 levels of transcriptional activity of those genes in round spermatids [red in Fig. 6A, transcription
243 data from (42, 43)].

244 We compared our BRD4 ChIP-seq data in round spermatids to previously published
245 BRDT ChIP-seq data from the same cell type (25). Although this previous study showed that
246 BRDT binds to the TSS of active genes in round spermatids, we found the majority of BRDT
247 peaks (~64%) to be present in intergenic regions of the genome and only 3% of peaks within
248 gene promoters (Fig. 5B). However, BRDT enrichment at gene promoters does correlate with
249 the transcriptional activity of those genes (Fig. 6A). These data suggest that while most BRDT
250 is found in intergenic regions, the small percentage located at gene promoters correlates well
251 with transcriptional activity.

252 Because both BRD4 and BRDT were found to bind to the promoters of active genes in
253 round spermatids, we sought to investigate possible differences between the roles of these BET
254 family proteins. We defined a list of genes bound by BRD4 based on the presence of peaks 1kb

upstream of the TSS. We then intersected this list with a list of approximately 1,544 genes previously shown to be bound by BRDT in round spermatids (25). Thus, we generated three categories of genes: BRD4-bound (approximately 2,093 genes), BRDT-bound (approximately 1,347 genes), and co-bound (approximately 197 genes). Genes bound only by BRD4 showed an average expression level that is slightly higher than genes bound only by BRDT (Fig. 6B). However, the average expression levels of BRD4- or BRDT-bound genes were approximately two-fold higher than the average expression level of all genes and similar to the average expression level of spermatogenesis-specific genes [$p < 2.2e^{-16}$ for BRD4- and BRDT-bound in (Fig. 6B)]. Interestingly, genes that were co-bound by BRD4 and BRDT show the highest average transcription level [$p < 2.2e^{-16}$ in (Fig. 6B)]. These same trends can be seen with levels of H3 and H4 acetylation at genes bound by BRD4, BRDT, or both (Fig. 6C). Histone H3/H4 acetylation levels are higher at the promoters of genes that are only bound by BRD4, but are highest at the promoters of genes that are co-bound by BRD4 and BRDT [see Table 2 for p-values in (Fig. 6B,C)]. As a control, H3K9me3 enrichment is extremely low at the promoters of genes bound by BRD4 and BRDT.

Next, we performed Gene Ontology (GO) analysis of BRD4-, BRDT-, or co-bound genes to determine if BRD4 and BRDT could possibly regulate different categories of genes. Categories of housekeeping genes such as “RNA processing” or “protein folding” can be found in genes bound by BRD4 or BRDT only (Fig. 6D,E left two panels). However, spermatogenesis-specific genes are enriched in the gene set bound by BRD4 only or co-bound by BRD4 and BRDT (Fig. 6D,E left and right panels). Indeed, heatmap analysis of BRD4 and BRDT enrichment at the TSS of all spermatogenesis-specific genes reveals a strong positioning of BRD4 (Fig. 6F). These data suggest that BRD4 and BRDT both play a role in the activation

of transcription in post-meiotic spermatids, but that BRD4 may play a particularly strong role in activation of spermatogenesis-specific genes.

The necessity of BRD4 in transcriptional activation during spermiogenesis is difficult to determine in the current absence of a conditional knockout mouse or reliable spermatogenic cell culture system. Knockdowns in the germline are extremely difficult to generate, and staged cell populations are not easily obtainable or manipulated in cell culture. Moreover, treatment of male mice with JQ1 results in a meiotic arrest, before spermiogenesis (26). Thus, currently we are unable to directly test the function of BRD4 during spermiogenesis.

BRD4 association with poly-acetylated histone H4 diminishes in late spermatids as acetylated histones are removed from the condensing nucleus

Although our ChIP-sequencing data provides correlative evidence of BRD4 binding to both acetylated histone H3 and H4, it does not demonstrate direct binding to these histone PTMs. To investigate the composition of BRD4-associated chromatin, we performed immunoprecipitation (IP) of BRD4 in round spermatids (Fig. 7A). Total cell lysate and BRD4-immunoprecipitated proteins were separated on an SDS-PAGE gel and analyzed with mass spectrometry. We quantified the fraction of peptides bearing different combinations of acetyl and methyl PTMs for histones H3 and H4 in total chromatin and BRD4-immunoprecipitated chromatin (Table 3). When the values of immunoprecipitated peptides were normalized to the values for total chromatin in round spermatids, we noticed an approximate 4- and 10-fold enrichment of tri- and tetra-acetylated H4 peptide, respectively (log-transformed ratios in Fig. 7A bottom left panel; see Table 3 for raw values). Specifically, various combinations of tri- and tetra-acetylated H4 peptides (K5, 8, 12, and 16ac) were highly enriched in immunoprecipitated

chromatin, but all these most highly enriched combinations include H4K5ac or H4K8ac (Fig. 7A right panel and Table 3). In general, H3K9ac is not enriched in BRD4-immunoprecipitated chromatin and H3K14ac is only slightly enriched when combined with different degrees of H3K9 methylation (Fig. 7A upper left panel). The reason for the relative absence of H3 acetylation and higher H3K9me3 is not clear.

We then quantified the change in total and BRD4-immunoprecipitated H4 acetylation over the course of spermatogenesis (raw values in Table 4). We generated ratios of H4 acetylation in round spermatids versus spermatocytes and compared these to the ratio of H4 acetylation in elongating/condensing spermatids versus round spermatids. First, tri- and tetra-acetylated H4 peptide levels increase significantly in total chromatin over the course of spermiogenesis (from spermatocytes to round spermatids to elongating/condensing spermatids) (Fig. 7B left graph). Although levels of BRD4-immunopreceipitated mono-, tri-, and tetra-acetylated H4 increase from spermatocytes to round spermatids, the levels of tetra-acetylated H4 decrease significantly from round spermatids to elongating/condensing spermatids (Fig. 7B right graph). Interestingly, the immunofluorescent signal of hyper-acetylated histones is depleted from the nuclear region underlying the acrosome (Movie D), as was shown in human spermatids (16), and adjacent to the BRD4 ring (Fig. 7C). Taken together, these data suggest a localization of BRD4 from the genome to the ring structure followed by removal of hyper-acetylated histones from the genome as the acrosome caps the nucleus (see model in Fig. 7D).

DISCUSSION

Mammalian spermatogenesis results in a specialized sperm cell with a highly compacted nucleus. A hallmark of this nuclear compaction is the removal of almost all histones from the

genome, with a small percentage retained at developmentally important loci (3, 4) and repetitive DNA sequences (7, 8). While the mechanism of mass histone removal and degradation remains unclear, it is believed that histone hyper-acetylation and thus, bromodomain-containing proteins, especially BRDT, are integral to this process (2, 20, 21, 25, 27). Surprisingly little is known about the involvement of the other BET family members – BRD2, BRD3, and BRD4 – during spermiogenesis. A previous study used immunohistochemistry of testes tissue to show BRD4 expression specifically in spermatogonia (30). In this study, however, we found that BRD4 is expressed during meiotic and post-meiotic phases of mouse spermatogenesis using several approaches. First, we detect BRD4 gene expression in meiotic and post-meiotic cells with western blotting and RT-qPCR (Fig. 1B and data not shown). Second, we immunoprecipitated BRD4 from meiotic and post-meiotic cells and detect its association with expressed genes and with acetylated histones [(44) and Figs. 5, 6, and 7]. Thus, BRD4 protein is present during the post-meiotic phase of spermatogenesis.

Our characterization of BRD4 in spermatids provides evidence for an interesting mechanism by which transcription is attenuated by the progressive removal of BRD4 itself and acetylated histones via the acrosome. It is possible that this might be a general mechanism for removal of transcriptionally relevant proteins. We initially observed BRD4 in a novel ring-like structure that is closely associated, both spatially and functionally, with the acrosome/acroplaxome. However, our unprecedented combination of IP/mass spectrometry and ChIP-seq analysis of BRD4 with endogenous antibodies demonstrate the *in vivo* binding of BRD4 throughout the chromatin of post-meiotic cells. Importantly, we performed these analyses in round spermatids, just before the BRD4 ring first appears and an increase in histone H4 acetylation can be detected by western blot, IF, and mass spectrometry (Figs. 1B, 2A,B and

7B). Also, in this cell type, we were able to capture the chromatin state before the initiation of histone replacement, vast compaction, and transcriptional shutdown.

BRD4 has traditionally been associated with euchromatin, active transcription, or mitotic bookmarking (45-51). Our ChIP-sequencing data suggest that BRD4 plays a similar role in transcriptional activation in round spermatids. BRD4, H3K9ac, and H4K5,8,12, and 16ac are present at the TSS of active genes in round spermatids, and their enrichment correlates with transcription levels (Figs. 5 and 6A). While BRD4 is known to bind to poly-acetylated histone H4 *in vitro*, our study is the first to confirm this preference for acetylated H4 (especially poly-acetylated H4 modified at K5 and K8) over H3 by *in vivo* IP/mass spectrometry using an antibody against endogenous BRD4 [Fig. 7A and (49, 52, 53)].

When we compared our ChIP-sequencing data to that published in a recent study of BRDT in the same cell type (25), we found that BRD4 and BRDT enrichment at gene promoters correlates with the transcriptional activity of those genes (Fig. 6A). BRD4 is especially enriched at spermatogenesis-specific genes and shows a very robust positioning around their TSS, suggesting that this BET family protein may play a strong role in their activation (Fig. 6F). Interestingly, genes that were co-bound by BRD4 and BRDT showed higher average transcription and histone acetylation levels than genes bound only by BRD4 or BRDT (Fig. 6B,C). It is unclear how BRD4, BRDT, or both would be recruited to specific subsets of genes, but these data suggest that synergistic binding of these two BET family proteins could lead to higher histone acetylation and expression levels via increased recruitment of the P-TEFb complex, as has been shown for both BRD4 and BRDT (25, 50, 51).

Although BRDT binds to a considerable number of gene promoters, we found that the majority of BRDT peaks occur in intergenic regions of the genome (Fig. 5B). Interestingly, a

Molecular and Cellular Biology

recent study demonstrated that nucleosomes that are retained in the mature mouse sperm genome show a ten-fold overrepresentation at promoter regions (54). Because BRDT has also been implicated in the histone-to-protamine transition via removal of acetylated histones, we propose that BRDT may show a binding preference for regions where histones are largely evicted from the mature sperm genome, perhaps even as early as the round spermatid stage (20, 23, 25). In the future, it will be interesting to investigate the genome-wide binding patterns of other BET family proteins over the course of spermatogenesis.

Because transcription is largely de-activated as the genome is highly compacted during spermiogenesis, it is reasonable to postulate that BRD4 and other transcriptional co-activators must be removed from the genome during this process. Indeed, western blot analysis shows that BRDT, BRD2, and BRD4 are largely absent from mature sperm (Fig. 1B). It is currently unclear, however, how histones and so many other chromatin components may be removed and/or degraded during this nuclear condensation. In approximately stage 7-8 spermatids, when histone hyperacetylation and nuclear elongating/compaction begin, the BRD4 ring appears just adjacent to the acroplaxome (Figs. 1B, 2B, 3C and Movies A-C). At the same stage of spermiogenesis, we observed by western blot a BRD4 peptide of a slightly lower molecular weight than the full length BRD4 isoform (Fig. 1B). It is possible that the BRD4 ring may contain a spermatid-specific isoform that binds to acetylated histones or other acetylated chromatin-associated proteins in order to provide a tethering force (via the acroplaxome) for chromatin compaction and reorganization. Indeed, a growing body of evidence implicates BRD4 in structural roles such as tethering, insulating, and maintaining higher order chromatin structure (55-58). Alternatively, because BRD4 is undetectable in mature sperm by IF and

Molecular and Cellular Biology

western blot, this smaller BRD4 peptide may simply be a degradation product that is created during the removal of BRD4 from the genome via the acroplaxome-associated ring.

Interestingly, the BRD4 ring does not form in acrosomal mutant mice, which show nuclear compaction and fertility defects that are highly similar to human globozoospermia, a condition in which the acrosome is malformed or absent, the sperm head is round, and chromatin compaction is abnormal [Fig. 4 and (11-15)]. Chromatin compaction during spermiogenesis may be incomplete in these mutant mice due to abnormal retention of chromatin-associated proteins and histones. Future ChIP-sequencing studies in acrosomal mutant mice will elucidate potential defects in the chromatin signature characteristic of spermiogenesis.

Our observations strongly support an increasing body of evidence that acrosome formation plays a key role in nuclear compaction and chromatin remodeling during spermiogenesis. Our IF data in mouse (Fig. 7C and Movie D) and that of a recent study in human spermatids shows that acetylated histones in the nucleus are depleted first in the region directly adjacent to the acrosome, where initial DNA compaction occurs (16). Moreover, various chromatin-associated proteins known to be involved in chromatin compaction, such as H1T2, are found in the nucleus adjacent to the acrosome (59). Finally, it has been suggested that the acroplaxome is able to provide contractile force to the compacting nucleus (10). It is unclear whether histones are degraded within the nucleus or shuttled out of the nucleus first during spermiogenesis; however, recent studies have shown that histone removal, while delayed, still occurs in mice lacking PA200, the acetylated histone-binding activator of the spermatogenesis-specific proteasome (21).

As histone removal followed by degradation appears to be the most supported model, the acroplaxome is in an ideal location to facilitate this potential shuttling (22). It has been shown that the nuclear membrane underlying the expanding acrosomal cap is devoid of any nuclear pores and may be impenetrable to exiting nuclear components (37). If the acrosome is coupled to the extensive removal of histones and other chromatin components from the genome, the force-providing acroplaxome could act to facilitate shuttling at the base of the acrosome where nuclear pores and lamins B1 and B3 are still present. Future studies, such as mass spectrometry analysis, will provide critical insight into potential binding partners or post-translational modifications of BRD4 that may localize this protein to the acroplaxome in spermatids. Regardless, this striking BRD4 localization suggests an interesting link between a chromatin component known to bind to acetylated histones and extra-nuclear spermatogenic structures.

Our combined approaches of immunofluorescence, biochemistry, mass spectrometry, and ChIP-sequencing suggest that BRD4 may play a fundamental role in transcription of spermatogenesis-specific genes and then in the transition from the transcriptionally active genome of early post-meiotic spermatids to the highly compact, transcriptionally silent genome of mature sperm. Importantly, our characterization of BRD4 contributes to the growing body of evidence that dramatic chromatin events taking place in the nucleus during spermiogenesis may be directly affected by extra-nuclear changes in cell structure and composition. Further investigation should reveal other proteins that are also involved in this process and elucidate the mechanism by which histones and other chromatin components are removed from the genome in an apparently acrosome-dependent manner. Finally, it would be interesting to further investigate how BET family proteins function during spermiogenesis to first activate transcription and then to repress it by potentially removing acetylated histones from the

spermatid genome. The future study of various steps in this intricate process of transcriptional repression and nuclear compaction will lead to a better understanding of chromatin dynamics during spermatogenesis, epigenetic signatures in sperm, and mammalian fertility.

MATERIALS AND METHODS

Antibodies/Reagents

Application	Antibodies/Reagents
Immunofluorescence	BRD2 (Abcam ab111078), BRD4 (60), BRDT (Abcam ab5157), H3K9Ac (Active Motif AM39137), H4K5,8,12,16ac (Millipore 05-1355), JQ1-PEG2-biotin (39), Lamin B1 (Abcam ab16048), Lamin B1 (Santa Cruz sc-373918), phalloidin-488 (Invitrogen A12379), and PNA-488 (Invitrogen L21409)
Western blot	β-actin (Cell Signalling 4970), BRD2 (Lifespan Biosciences (aa524-573) IHC-plus LS-B923), BRD4 (60), BRDT (Abcam ab5157), Cyclin T1 (Santa Cruz H245 sc-10750), GAPDH (Fitzgerald 10R-G109a), H3K9Ac (Active Motif AM39137), H4 (Abcam ab10158), H4K5ac (Millipore 07-327), H4K8Ac (Millipore 07-328), H4K12Ac (Millipore 07-595), H4K16Ac (Active Motif AM39167), H4K5,8,12,16ac (Millipore 05-1355)
Immunoprecipitation/ ChIP	H3 (Abcam ab1791), H3K9ac (Active Motif AM39137), H3K9me3 (Abcam ab8898), H4K5ac (Millipore 07-327), H4K8ac (Millipore 07-328), H4K12ac (Millipore 07-595), H4K16ac (Active Motif AM39167), H4K5,8,12,16ac (Millipore 06-866), BRD4 (Bethyl A301-985A50)

Mouse Models

Male 129S6/SvEvTac mice (Taconics, Germantown, NY) as well as *Hrb*$^{-/-}$ gene-disrupted mice (11) were maintained and humanely euthanized according to the guidelines of the University of Pennsylvania Institutional Animal Care and Use Committee.

Mouse spermatogenic cell fractionation

Spermatogenic cell fractionation was performed by sedimentation of cells prepared from adult mouse testes through a BSA gradient as previously described (33). Each fractionation experiment used approximately 22 testes. Fractions were analyzed for purity based on cell and nuclear morphology (via DAPI staining) and pooled. Mature spermatozoa were obtained from epididymides of adult mice, and contaminating cell types were eliminated by incubating in somatic cell lysis buffer (0.1% SDS, 0.5% Triton X-100 in DEPC H_2O) on ice for 20 minutes.

Western blot analysis

Cells were resuspended in buffer [20mM TrispH 7.5, 1mM $MgCl_2$, 1mM $CaCl_2$, 137mM NaCl, 10%Glycerol, 1% NP-40, Complete protease inhibitor EDTA-free (Roche), 300nM trichostatin A (Sigma T1952)], and rotated at 4°C for one hour in the presence of 12.5 U/mL Benzonase (Novagen 70746). Protein content was measured with Bradford dye and cell lysate containing 25µg of protein or sperm lysate containing 5µg of protein was added to each well of a 4-12% 1mm Bis-Tris NuPAGE protein gel. Protein was transferred to a PVDF membrane and blocked for one hour in 5% BSA-TBST. Membranes were incubated with primary antibody (in 1% BSA-TBST) for one hour, washed, incubated with secondary HRP-conjugated antibody (in 1% BSA-TBST) for 30 minutes, washed, and detected using enhanced chemiluminescence. For peptide competition, primary antibody was incubated with 5µg/mL immunizing peptide for one hour at room temperature before application to the membrane.

Immunofluorescence

Immunofluorescence was performed on 8µm cryosections of mouse testes from ten-week-old mice or cell suspensions obtained using the spermatogenic cell separation method described

above (33). Testes were dissected and immediately placed in 4% PFA (in PBS) or snap frozen in liquid nitrogen. The PFA-fixed testes were incubated in 15%, then 30% sucrose (in PBS) and embedded in TissueTek OCT compound. Fixed or frozen tissue was cryosectioned onto Superfrost Plus slides (Fisher). Cell suspensions in PBS were allowed to adhere to Superfrost Plus slides for 1hr at 33°C. Snap frozen sections and cell suspensions were fixed for 15min in 4% paraformaldehyde at room temperature. Sections/cells were washed 3 x 5min in PBS and incubated with 125mM glycine (in PBS) for one minute at room temperature. Sections/cells were washed 3 x 5 min in PBS, then permeabilized with 0.1% Triton-X100 for two minutes at 4°C. Sections/cells were washed 3 x 5 min in PBS, then blocked with 3% donkey serum in PBS for one hour at 37°C. Sections/cells were incubated with primary antibody or 40μM JQ1-biotin (in 3% donkey serum in PBS) for one hour at 37°C and washed 3 x 5 min in PBS. Sections/cells were incubated with 5μg/mL (in 3% donkey serum in PBS) Alexafluor secondary antibody (Invitrogen) for 30min at 37°C, then washed 3 x 5min in PBS. Sections/cells were then incubated with DAPI (Invitrogen, 5μg/mL in 3% donkey serum in PBS) and embedded in Prolong Gold Anti-fade reagent (Invitrogen). Sections/cells were imaged with a Leica TCS SP8 confocal microscope and pseudo-3D images were created using Velocity 6 software. Minimal changes to immunofluorescence images (contrast and pseudo-coloring) were made using ImageJ.

Chromatin immunoprecipitation and sequencing

ChIP-seq for BRD4 and histone post-translational modifications was carried out as previously described with minor modifications (61). Cells were cross-linked in 1% formaldehyde in PBS for 10 minutes at room temperature. The reaction was quenched with 125mM glycine in PBS

Molecular and Cellular Biology

for five minutes at room temperature. After cell lysis, lysates were sonicated for 20 minutes with a Covaris S220 sonicator (5% duty cycle, 140 watts peak incident power, 200 cycles per burst). For each IP, 500µg of protein (measured with BCA assay) from the cell lysate, 30µL protein G Dynabeads (Life Technologies), and 5µg-10µg of antibody or IgG (Pierce 31235) were used. ChIP libraries for sequencing were prepared using 5ng DNA and the NEBNext Ultra DNA library prep kit for Illumina. Size selection was performed using AMPure XP beads (Beckman Coulter, Inc. #A63881). Libraries were sequenced using a NextSeq 500 machine (Illumina) as per manufacturer's protocols.

ChIP-seq data analysis

ChIP-seq data generated using a NextSeq 500 were demultiplexed using the bcl2fastq utility (02.14.01.07). Data were then aligned using bowtie 0.12.7 (parameters -m 1 --best) to mouse genomic assembly mm9.

UCSC Genome Browser Tracks

Visual tracks of ChIP-seq data were generated in the following way. For each sample, the aligned data file for PCR duplicated reads was filtered (i.e., any set of aligned reads with the same chromosome, start, and stop coordinates was reduced to a single representative). Coverage maps were then created using the BEDTools utility genomeCoverageBed. Resulting bedGraphs were scaled using the RPKM coefficient, a measure of the number of billions of bases sequenced per sample, to correct for sequencing efficiency biases. Finally, an input coverage map was subtracted for the BRD4 and each histone PTM coverage map. The BRDT data from (25) were treated similarly.

Genome Compartment Plot

The genomic compartment table was generated by first calling peaks for each histone PTM or BRD4 using SICER (peaks were called against input as the background; window, fragment, and gap size parameters were fixed at 200bp; and the FDR was controlled at 0.1%). Previously published peak locations from (25) were used for BRDT. Peak locations were overlapped using BEDTools' intersect utility with RefSeq promoters, exons, and introns, in an exclusive way: if a peak overlapped a promoter, it was removed from consideration for overlap with exons or introns, and if it overlapped an exon it was removed from consideration for overlap with introns.

Expression versus ChIP Enrichment Heatmap

RefSeq transcripts were assessed for expression in round spermatids by loading two previously published replicate data sets (GSM95950 and GSM95951 in GEO series GSE4193) into the Partek Genomics Suite software package. Data were background-corrected with GC-RMA, quantile-normalized, and median polished along with all other data sets in the GSE4193 series. Promoters (1kb upstream regions) associated with these expression-scored transcripts were assessed for numbers of aligned tags in each indicated ChIP. Tag counts were then normalized to the number of millions of tags sequenced as well as input. Brightness for each track is scaled to the maximum ChIP value in that track; tracks are sorted in order of least expressed to most expressed genes in GSM95950.

Expression Boxplots

BRDT target genes are as described in (25). BRD4 target genes were those with a SICER-determined BRD4 peak in the promoter where the peak enrichment was in the 90th percentile of all BRD4 peaks. For each of the three gene sets, expression enrichments were determined using GSM95950 (data processing described above) and ChIP-seq enrichments were determined using normalized tag counts at the promoter (data processing described above). Table 2 p-values and

W statistics (reflecting expression distribution and promoter acetylation distribution differences between genes bound by BRD4, BRDT, both, or neither) were estimated using the one-sided Mann-Whitney test in R.

Gene Ontology Pie Charts

Gene Ontology enrichment analysis of BRD4 target genes, BRDT target genes, and co-bound genes was done using DAVID (62). GO terms in the "Biological Process" hierarchy were collapsed to a single representative term if they shared the same gene; if one GO term's associated target genes were a subset of another's, that GO term was dropped in favor of the other. GO terms were further combined if they shared more than 15 transcripts. GO terms are represented by their overall gene "real estate." Each gene is given a vote inversely proportional to the number of terms it appears in. Each term's weight is the sum of the votes of its genes. Finally, pie charts were simplified by visual inspection.

Promoter Heatmap

Genes enriched in the Gene Ontology category "Spermatogenesis" (GO:0007283) were associated with RefSeq transcripts using UniProt and DAVID. For each transcript, a vector describing the ChIP-seq enrichment profile around the TSS (2.5kb upstream and 2.5kb downstream) was assessed for BRD4 and BRDT (ChIP-seq enrichment data were normalized to input, length, and number of millions of reads, as above). Profiles were sorted top-to-bottom by overall BRD4 enrichment intensity. The maximum green in each plot was determined by the enrichment value at the 90th percentile.

Immunoprecipitation and mass spectrometry

Antibody-coupled beads were prepared by incubating 30µL/IP protein G Dynabeads (Life Technologies) with 10µg primary antibody or rabbit IgG (Pierce 31235) in 0.5% BSA-PBS for six hours at 4°C with rotation. Cells were resuspended in lysis buffer (20mM Tris pH 7.5, 1mM $MgCl_2$, 1mM $CaCl_2$, 137mM NaCl, 10% glycerol, 1% NP-40, Complete Protease inhibitor EDTA-free (Roche), 10mM NaB, 300nM Trichostatin A), after which 12.5 U/mL Benzonase was added. Lysates were incubated for one hour at 4°C with rotation and then cleared by centrifugation at 14,000 rpm for 10 minutes. Supernatant was removed and protein concentration was measured with Bradford dye. After incubating with antibody, beads were washed three times with 1mL buffer. One mg protein from the lysate was added to the beads and incubated overnight at 4°C with rotation. Beads were washed five times with 1mL buffer. Beads were resuspended in 30µL sample buffer and incubated for five minutes at 90°C. Eluate was separated from the beads, separated on a 4-12% 1mm Bis-Tris NuPAGE protein gel, and analyzed for enriched histone modifications compared to input samples with mass spectrometry (MS).

In-gel histone proteins were derivatized twice with a mixture of propionic anhydride and 100 mM ammonium bicarbonate (1:1) for 15 min under vigorous vortexing and then digested with 12.5 ng/µL of trypsin at room temperature overnight. Resultant histone peptides were extracted from the gel, re-propionylated twice, and then desalted using C18-based homemade stage-tips before MS analysis. Desalted peptides were separated by reverse phase nanospray liquid chromatography with the Thermo Scientific Easy-nLC 1000 system and an in-house packed C_{18} resin column (15cm in length and 3µm in particle size). Buffer A is water with 0.1% formic acid. Buffer B is acetonitrile with 0.1% formic acid. Histone peptides were eluted by a gradient from 2% to 30% of buffer B for 35 min, 30% to 98% of buffer B for 20 min followed

by a wash at 98% of buffer B for 15min with a flow rate of 200 nL/min. Mass spectrometry was performed on a Thermo Scientific Orbitrap Velos Pro hybrid ion trap-Orbitrap mass spectrometer. Each cycle includes one full MS scan (m/z 290 to 1400, resolution of 60,000, AGC target value of $1x10^6$), followed by seven data-dependent MS2 scans of the most intense peptide ions using CID (normalized collision energy of 35%, isolation width of 3 m/z, AGC target value of $1x10^4$). In the section between 23 min and 45 min, MS2 scans targeting precursor ions with m/z of 528.30, 570.84, 768.95, 761.94 and 754.93 (isolation width of 1 m/z) were performed for the determination of acetylation sites on histone peptides with multiple lysines. Dynamic exclusion of 25 s was used to prevent repeated analysis of the same components. Ions with a charge state of one or more than four and a rejection list of common contaminant ions were excluded from the analysis. Histone peptides were identified based on retention times and tandem MS. Abundance of histone peptides were quantified by integrating the area under each peak in the MS chromatogram using Thermo Scientific Xcalibur Qual Browser. The LC-MS/MS data sets were also analyzed using in-house developed software as previously described (49).

ACKNOWLEDGEMENTS

We thank the members of the Berger lab, especially Dr. Parisha Shah, for all their support and advice. We thank Dr. Jérôme Govin for his guidance. We thank Dr. Saadi Khochbin for his advice and sharing his BRDT ChIP-seq data. We thank Dr. Jan Van Deursen for sharing his *Hrb*$^{-/-}$ mice. We thank Dr. James Bradner for sharing JQ1-biotin. We thank Andrea Stout of the Cell and Developmental microscopy core for her help with the

immunofluorescence imaging. We thank Joseph Grubb and Jonathan Schug of the University of Pennsylvania Functional Genomics Core for their help with ChIP sequencing.

Support to JMB was from the T32 Genetics Training Grant at the University of Pennsylvania (GM008216). Support to SLB was from NIH grants GM055360 and U54-HD068157. BAG acknowledges funding from NIH grant GM110174 and Innovator grant (DP2OD007447) from the Office of the Director. RGM was supported by NIH grants R01HD048837 and U54HD068157.

DISCLOSURES

The authors declare that they have no competing financial interests. All experiments requiring the use of laboratory mice were executed in compliance with all relevant guidelines, regulations and regulatory agencies. Mouse experiments were conducted under the guidance and approval of the University of Pennsylvania institutional animal care and use committee.

REFERENCES

1. **Rajender S, Avery K, Agarwal A.** 2011. Epigenetics, spermatogenesis and male infertility. Mutation Research/Reviews in Mutation Research **727:**62-71.
2. **Govin J, Caron C, Lestrat C, Rousseaux S, Khochbin S.** 2004. The role of histones in chromatin remodelling during mammalian spermiogenesis. European Journal of Biochemistry **271:**3459-3469.
3. **Brykczynska U, Hisano M, Erkek S, Ramos L, Oakeley EJ, Roloff TC, Beisel C, Schubeler D, Stadler MB, Peters AH.** 2010. Repressive and active histone methylation

mark distinct promoters in human and mouse spermatozoa. Nat Struct Mol Biol **17:**679-687.

4. **Hammoud SS, Nix DA, Zhang H, Purwar J, Carrell DT, Cairns BR.** 2009. Distinctive chromatin in human sperm packages genes for embryo development. Nature **460:**473-478.

5. **Arpanahi A, Brinkworth M, Iles D, Krawetz SA, Paradowska A, Platts AE, Saida M, Steger K, Tedder P, Miller D.** 2009. Endonuclease-sensitive regions of human spermatozoal chromatin are highly enriched in promoter and CTCF binding sequences. Genome Research **19:**1338-1349.

6. **Carone BR, Hung JH, Hainer SJ, Chou MT, Carone DM, Weng Z, Fazzio TG, Rando OJ.** 2014. High-resolution mapping of chromatin packaging in mouse embryonic stem cells and sperm. Dev Cell **30:**11-22.

7. **Meyer-Ficca ML, Lonchar JD, Ihara M, Bader JJ, Meyer RG.** 2013. Alteration of poly(ADP-ribose) metabolism affects murine sperm nuclear architecture by impairing pericentric heterochromatin condensation. Chromosoma **122:**319-335.

8. **Samans B, Yang Y, Krebs S, Sarode GV, Blum H, Reichenbach M, Wolf E, Steger K, Dansranjavin T, Schagdarsurengin U.** 2014. Uniformity of nucleosome preservation pattern in Mammalian sperm and its connection to repetitive DNA elements. Dev Cell **30:**23-35.

9. **Gaucher J, Reynoird N, Montellier E, Boussouar F, Rousseaux S, Khochbin S.** 2010. From meiosis to postmeiotic events: The secrets of histone disappearance. FEBS Journal **277:**599-604.

10. **Kierszenbaum AL, Tres LL.** 2004. The acrosome-acroplaxome-manchette complex and the shaping of the spermatid head. Arch Histol Cytol **67:**271-284.

11. **Kang-Decker N, Mantchev GT, Juneja SC, McNiven MA, van Deursen JM.** 2001. Lack of acrosome formation in Hrb-deficient mice. Science **294:**1531-1533.

12. **Fujihara Y, Satouh Y, Inoue N, Isotani A, Ikawa M, Okabe M.** 2012. SPACA1-deficient male mice are infertile with abnormally shaped sperm heads reminiscent of globozoospermia. Development **139:**3583-3589.

13. **Lin YN, Roy A, Yan W, Burns KH, Matzuk MM.** 2007. Loss of zona pellucida binding proteins in the acrosomal matrix disrupts acrosome biogenesis and sperm morphogenesis. Molecular and Cellular Biology **27:**6794-6805.

14. **Xiao N, Kam C, Shen C, Jin W, Wang J, Lee KM, Jiang L, Xia J.** 2009. PICK1 deficiency causes male infertility in mice by disrupting acrosome formation. J Clin Invest **119:**802-812.

15. **Yao R, Ito C, Natsume Y, Sugitani Y, Yamanaka H, Kuretake S, Yanagida K, Sato A, Toshimori K, Noda T.** 2002. Lack of acrosome formation in mice lacking a Golgi protein, GOPC. Proc Natl Acad Sci U S A **99:**11211-11216.

16. **De Vries M, Ramos L, Housein Z, De Boer P.** 2012. Chromatin remodelling initiation during human spermiogenesis. Biology Open **1:**446-457.

17. **Grimes SR, Jr., Henderson N.** 1984. Hyperacetylation of histone H4 in rat testis spermatids. Exp Cell Res **152:**91-97.

18. **Meistrich ML, Trostle-Weige PK, Lin R, Bhatnagar YM, Allis CD.** 1992. Highly acetylated H4 is associated with histone displacement in rat spermatids. Mol Reprod Dev **31:**170-181.

19. **Govin J, Escoffier E, Rousseaux S, Kuhn L, Ferro M, Thevenon J, Catena R, Davidson I, Garin J, Khochbin S, Caron C.** 2007. Pericentric heterochromatin reprogramming by new histone variants during mouse spermiogenesis. The Journal of Cell Biology **176:**283-294.

20. **Shang E, Nickerson HD, Wen D, Wang X, Wolgemuth DJ.** 2007. The first bromodomain of Brdt, a testis-specific member of the BET sub-family of double-bromodomain-containing proteins, is essential for male germ cell differentiation. Development **134:**3507-3515.

21. **Qian MX, Pang Y, Liu CH, Haratake K, Du BY, Ji DY, Wang GF, Zhu QQ, Song W, Yu Y, Zhang XX, Huang HT, Miao S, Chen LB, Zhang ZH, Liang YN, Liu S, Cha H, Yang D, Zhai Y, Komatsu T, Tsuruta F, Li H, Cao C, Li W, Li GH, Cheng Y, Chiba T, Wang L, Goldberg AL, Shen Y, Qiu XB.** 2013. Acetylation-mediated proteasomal degradation of core histones during DNA repair and spermatogenesis. Cell **153:**1012-1024.

22. **Goudarzi A, Shiota H, Rousseaux S, Khochbin S.** 2014. Genome-Scale Acetylation-Dependent Histone Eviction during Spermatogenesis. J Mol Biol.

23. **Pivot-Pajot C, Caron C, Govin J, Vion A, Rousseaux S, Khochbin S.** 2003. Acetylation-Dependent Chromatin Reorganization by BRDT, a Testis-Specific Bromodomain-Containing Protein. Molecular and Cellular Biology **23:**5354-5365.

24. **Bryant JM, Berger SL.** 2012. Low-hanging fruit: targeting Brdt in the testes. EMBO J **31:**3788-3789.

25. **Gaucher J, Boussouar F, Montellier E, Curtet S, Buchou T, Bertrand S, Hery P, Jounier S, Depaux A, Vitte A-L, Guardiola P, Pernet K, Debernardi A, Lopez F,**

Holota H, Imbert J, Wolgemuth DJ, Gérard M, Rousseaux S, Khochbin S. 2012. Bromodomain-dependent stage-specific male genome programming by Brdt. The EMBO Journal **31:**3809-3820.

26. **Matzuk Martin M, McKeown Michael R, Filippakopoulos P, Li Q, Ma L, Agno Julio E, Lemieux Madeleine E, Picaud S, Yu Richard N, Qi J, Knapp S, Bradner James E.** 2012. Small-Molecule Inhibition of BRDT for Male Contraception. Cell **150:**673-684.

27. **Berkovits BD, Wolgemuth DJ.** 2011. The first bromodomain of the testis-specific double bromodomain protein Brdt is required for chromocenter organization that is modulated by genetic background. Developmental Biology **360:**358-368.

28. **Shang E, Wang X, Wen D, Greenberg DA, Wolgemuth DJ.** 2009. Double bromodomain-containing gene Brd2 is essential for embryonic development in mouse. Developmental Dynamics **238:**908-917.

29. **Houzelstein D, Bullock SL, Lynch DE, Grigorieva EF, Wilson VA, Beddington RSP.** 2002. Growth and Early Postimplantation Defects in Mice Deficient for the Bromodomain-Containing Protein Brd4 Molecular and Cellular Biology **22:**3794-3802.

30. **Shang E, Salazar G, Crowley TE, Wang X, Lopez RA, Wang X, Wolgemuth DJ.** 2004. Identification of unique, differentiation stage-specific patterns of expression of the bromodomain-containing genes Brd2, Brd3, Brd4, and Brdt in the mouse testis. Gene Expression Patterns **4:**513-519.

31. **Voigt P, Reinberg D.** 2011. BRD4 jump-starts transcription after mitotic silencing. Genome Biology **12:**133.

32. **McBride AA, Jang MK.** 2013. Current understanding of the role of the Brd4 protein in the papillomavirus lifecycle. Viruses **5:**1374-1394.

33. **Bryant JM, Meyer-Ficca ML, Dang VM, Berger SL, Meyer RG.** 2013. Separation of spermatogenic cell types using STA-PUT velocity sedimentation. J Vis Exp.

34. **Meistrich ML, Hess RA.** 2013. Assessment of spermatogenesis through staging of seminiferous tubules. Methods Mol Biol **927:**299-307.

35. **Schutz W, Alsheimer M, Ollinger R, Benavente R.** 2005. Nuclear envelope remodeling during mouse spermiogenesis: postmeiotic expression and redistribution of germline lamin B3. Exp Cell Res **307:**285-291.

36. **Vester B, Smith A, Krohne G, Benavente R.** 1993. Presence of a nuclear lamina in pachytene spermatocytes of the rat. J Cell Sci **104 (Pt 2):**557-563.

37. **Ho HC.** 2010. Redistribution of nuclear pores during formation of the redundant nuclear envelope in mouse spermatids. J Anat **216:**525-532.

38. **Filippakopoulos P, Qi J, Picaud S, Shen Y, Smith WB, Fedorov O, Morse EM, Keates T, Hickman TT, Felletar I, Philpott M, Munro S, McKeown MR, Wang Y, Christie AL, West N, Cameron MJ, Schwartz B, Heightman TD, La Thangue N, French CA, Wiest O, Kung AL, Knapp S, Bradner JE.** 2010. Selective inhibition of BET bromodomains. Nature **468:**1067-1073.

39. **Anders L, Guenther MG, Qi J, Fan ZP, Marineau JJ, Rahl PB, Loven J, Sigova AA, Smith WB, Lee TI, Bradner JE, Young RA.** 2014. Genome-wide localization of small molecules. Nat Biotechnol **32:**92-96.

40. **Abou-Haila A, Tulsiani DR.** 2000. Mammalian sperm acrosome: formation, contents, and function. Arch Biochem Biophys **379:**173-182.

41. **Kierszenbaum AL, Tres LL, Rivkin E, Kang-Decker N, van Deursen JM.** 2004. The acroplaxome is the docking site of Golgi-derived myosin Va/Rab27a/b- containing proacrosomal vesicles in wild-type and Hrb mutant mouse spermatids. Biol Reprod **70:**1400-1410.

42. **Mulugeta Achame E, Wassenaar E, Hoogerbrugge JW, Sleddens-Linkels E, Ooms M, Sun ZW, van IWF, Grootegoed JA, Baarends WM.** 2010. The ubiquitin-conjugating enzyme HR6B is required for maintenance of X chromosome silencing in mouse spermatocytes and spermatids. BMC Genomics **11:**367.

43. **Namekawa SH, Park PJ, Zhang LF, Shima JE, McCarrey JR, Griswold MD, Lee JT.** 2006. Postmeiotic sex chromatin in the male germline of mice. Curr Biol **16:**660-667.

44. **Loven J, Hoke HA, Lin CY, Lau A, Orlando DA, Vakoc CR, Bradner JE, Lee TI, Young RA.** 2013. Selective inhibition of tumor oncogenes by disruption of super-enhancers. Cell **153:**320-334.

45. **Dey A, Nishiyama A, Karpova T, McNally J, Ozato K.** 2009. Brd4 Marks Select Genes on Mitotic Chromatin and Directs Postmitotic Transcription. Molecular Biology of the Cell **20:**4899-4909.

46. **Mochizuki K, Nishiyama A, Jang MK, Dey A, Ghosh A, Tamura T, Natsume H, Yao H, Ozato K.** 2008. The Bromodomain Protein Brd4 Stimulates G1 Gene Transcription and Promotes Progression to S Phase. Journal of Biological Chemistry **283:**9040-9048.

47. **Yang Z, He N, Zhou Q.** 2007. Brd4 Recruits P-TEFb to Chromosomes at Late Mitosis To Promote G1 Gene Expression and Cell Cycle Progression. Molecular and Cellular Biology **28:**967-976.

48. **Zuber J, Shi J, Wang E, Rappaport AR, Herrmann H, Sison EA, Magoon D, Qi J, Blatt K, Wunderlich M, Taylor MJ, Johns C, Chicas A, Mulloy JC, Kogan SC, Brown P, Valent P, Bradner JE, Lowe SW, Vakoc CR.** 2011. RNAi screen identifies Brd4 as a therapeutic target in acute myeloid leukaemia. Nature **478:**524-528.

49. **Leroy G, Chepelev I, Dimaggio PA, Blanco MA, Zee BM, Zhao K, Garcia BA.** 2012. Proteogenomic characterization and mapping of nucleosomes decoded by Brd and HP1 proteins. Genome Biology **13:**R68.

50. **Jang MK, Mochizuki K, Zhou M, Jeong HS, Brady JN, Ozato K.** 2005. The bromodomain protein Brd4 is a positive regulatory component of P-TEFb and stimulates RNA polymerase II-dependent transcription. Molecular Cell **19:**523-534.

51. **Yang Z, Yik JH, Chen R, He N, Jang MK, Ozato K, Zhou Q.** 2005. Recruitment of P-TEFb for stimulation of transcriptional elongation by the bromodomain protein Brd4. Molecular Cell **19:**535-545.

52. **Liu Y, Wang X, Zhang J, Huang H, Ding B, Wu J, Shi Y.** 2008. Structural basis and binding properties of the second bromodomain of Brd4 with acetylated histone tails. Biochemistry **47:**6403-6417.

53. **Dey A, Chitsaz F, Abbasi A, Misteli T, Ozato K.** 2003. The double bromodomain protein Brd4 binds to acetylated chromatin during interphase and mitosis. Proc Natl Acad Sci U S A **100:**8758-8763.

789 54. **Erkek S, Hisano M, Liang CY, Gill M, Murr R, Dieker J, Schubeler D, van der**
790 **Vlag J, Stadler MB, Peters AH.** 2013. Molecular determinants of nucleosome retention
791 at CpG-rich sequences in mouse spermatozoa. Nat Struct Mol Biol **20:**868-875.
792 55. **You J, Croyle JL, Nishimura A, Ozato K, Howley PM.** 2004. Interaction of the
793 bovine papillomavirus E2 protein with Brd4 tethers the viral DNA to host mitotic
794 chromosomes. Cell **117:**349-360.
795 56. **Baxter MK, McPhillips MG, Ozato K, McBride AA.** 2005. The mitotic chromosome
796 binding activity of the papillomavirus E2 protein correlates with interaction with the
797 cellular chromosomal protein, Brd4. Journal of Virology **79:**4806-4818.
798 57. **Floyd SR, Pacold ME, Huang Q, Clarke SM, Lam FC, Cannell IG, Bryson BD,**
799 **Rameseder J, Lee MJ, Blake EJ, Fydrych A, Ho R, Greenberger BA, Chen GC,**
800 **Maffa A, Del Rosario AM, Root DE, Carpenter AE, Hahn WC, Sabatini DM, Chen**
801 **CC, White FM, Bradner JE, Yaffe MB.** 2013. The bromodomain protein Brd4
802 insulates chromatin from DNA damage signalling. Nature **498:**246-250.
803 58. **Wang R, Li Q, Helfer CM, Jiao J, You J.** 2012. Bromodomain Protein Brd4
804 Associated with Acetylated Chromatin Is Important for Maintenance of Higher-order
805 Chromatin Structure. Journal of Biological Chemistry **287:**10738-10752.
806 59. **Martianov I, Brancorsini S, Catena R, Gansmuller A, Kotaja N, Parvinen M,**
807 **Sassone-Corsi P, Davidson I.** 2005. Polar nuclear localization of H1T2, a histone H1
808 variant, required for spermatid elongation and DNA condensation during
809 spermiogenesis. Proc Natl Acad Sci U S A **102:**2808-2813.
810 60. **Lamonica JM, Deng W, Kadauke S, Campbell AE, Gamsjaeger R, Wang H, Cheng**
811 **Y, Billin AN, Hardison RC, Mackay JP, Blobel GA.** 2011. Bromodomain protein

Brd3 associates with acetylated GATA1 to promote its chromatin occupancy at erythroid target genes. Proc Natl Acad Sci U S A **108:**E159-168.

61. **Shah PP, Donahue G, Otte GL, Capell BC, Nelson DM, Cao K, Aggarwala V, Cruickshanks HA, Rai TS, McBryan T, Gregory BD, Adams PD, Berger SL.** 2013. Lamin B1 depletion in senescent cells triggers large-scale changes in gene expression and the chromatin landscape. Genes & Development **27:**1787-1799.

62. **Huang da W, Sherman BT, Lempicki RA.** 2009. Systematic and integrative analysis of large gene lists using DAVID bioinformatics resources. Nat Protoc **4:**44-57.

TABLES

Table 1: ChIP-seq data alignment information

Total aligned reads compared to uniquely-mapped reads for each ChIP-seq sample

ChIP	Total Reads	Aligned Reads	Unique Reads	% Aligned	% Unique	% Genome Coverage
Input	54990464	35623672	32940684	64.78	92.47	90.64
H3	71828757	37798741	30151960	52.62	79.77	82.96
H3K9me3	84339867	39799707	27591619	47.19	69.33	75.92
H3K9ac	67856707	48595679	34042406	71.62	70.05	93.67
H4K5ac	66596815	46239262	34065138	69.43	73.67	93.73
H4K8ac	79795471	48838021	29541448	61.20	60.49	81.28
H4K12ac	71252246	46341541	33485169	65.04	72.26	92.14
H4K16ac	77287145	49326598	28973938	63.82	58.74	79.72
H4ac	70049830	48662721	32799658	69.47	67.40	90.25
BRD4	84730635	47671985	24864246	56.26	52.16	68.41

Table 2: Calculation of significant differences for Figures 6B and C

Figure 6B

Comparison of BRD4-, BRDT-, or co-bound gene expression

Test	W Statistic	p-value
BRD4 vs. All Genes	W = 2683292	p < 2.2e-16
BRDT vs. All Genes	W = 1729944	p < 2.2e-16

Co-bound vs. All Genes	W = 378363	p < 2.2e-16
Co-bound vs. BRD4	W = 181821	p = 2.6e-08
Co-bound vs. BRDT	W = 127587	p = 6.8e-11

Figure 6C

Comparison of BRD4-, BRDT-, or co-bound gene promoter acetylation level

Test	Histone PTM	W Statistic	p-value
BRD4 vs. BRDT	H3K9ac	W = 1403278	p < 2.2e-16
BRD4 vs. BRDT	H4K5ac	W = 1484792	p < 2.2e-16
BRD4 vs. BRDT	H4K8ac	W = 1466692	p < 2.2e-16
BRD4 vs. BRDT	H4K12ac	W = 1468998	p < 2.2e-16
BRD4 vs. BRDT	H4K16ac	W = 1444708	p < 2.2e-16
BRD4 vs. BRDT	H4Kac	W = 1479768	p < 2.2e-16
Co-bound vs. BRD4	H3K9ac	W = 276948.5	p = 7.411e-16
Co-bound vs. BRDT	H3K9ac	W = 158058	p < 2.2e-16
Co-bound vs. BRD4	H4K5ac	W = 273017.5	p = 2.435e-14
Co-bound vs. BRDT	H4K5ac	W = 162835.5	p < 2.2e-16
Co-bound vs. BRD4	H4K8ac	W = 277942.5	p = 2.972e-16
Co-bound vs. BRDT	H4K8ac	W = 162476.5	p < 2.2e-16
Co-bound vs. BRD4	H4K12ac	W = 272689	p = 3.232e-14
Co-bound vs. BRDT	H4K12ac	W = 161513.5	p < 2.2e-16
Co-bound vs. BRD4	H4K16ac	W = 271330.5	p = 1.027e-13
Co-bound vs. BRDT	H4K16ac	W = 158641.5	p < 2.2e-16
Co-bound vs. BRD4	H4Kac	W = 277562	p = 4.223e-16
Co-bound vs. BRDT	H4Kac	W = 162543	p < 2.2e-16

Table 3: Mass spectrometry analysis of BRD4-immunoprecipitated histones from round spermatids

Quantification of the degree of acetylation or methylation of histone H3 (amino acids 9 to 17, KSTGGKAPR) or H4 peptide (amino acids 4 to 17, GKGGKGLGKGGAKR). Shown are average ratios of the percentage of peptide of H3 or H4 in BRD4-immunoprecipitated chromatin to total chromatin. Standard deviation is calculated for two and four biological replicates for H3 and H4, respectively.

Peptide	AVG IP/Total	St Dev (±)
H3 9-17		
Unmodified	1.02	0.18

H3K9me1	0.65	0.28
H3K9me2	1.26	0.73
H3K9me3	4.24	1.51
H3K9ac	1.11	1.58
H3K14ac	1.09	0.08
H3K9me1K14ac	0.09	0.13
H3K9me2K14ac	1.35	1.09
H3K9me3K14ac	3.04	2.97
H3K9,14ac	0.00	0.00
H4 4-17		
Unmodified	1.14	0.20
H4Kac1	0.61	0.12
H4Kac2	0.98	0.08
H4Kac3	3.72	1.04
H4Kac4	10.07	5.17
Unmodified	1.17	0.21
H4K5ac	3.31	2.85
H4K8ac	2.67	4.89
H4K12ac	0.48	0.51
H4K16ac	0.87	0.42
H4K5,8ac	2.54	0.96
H4K5,12ac	1.36	0.87
H4K5,16ac	0.99	0.33
H4K8,12ac	0.83	0.35
H4K8,16ac	0.85	0.24
H4K12,16ac	0.80	0.13
H4K5,8,12ac	3.73	2.69
H4K5,8,16ac	4.18	1.51
H4K5,12,16ac	3.30	2.68
H4K8,12,16ac	2.82	1.54
H4K5,8,12,16ac	10.93	6.10

Table 4: Mass spectrometry analysis of BRD4-immunoprecipitated H4 during spermatogenesis

Quantification of the degree of acetylation (% total peptide) of histone H4 peptide (amino acids 4 to 17, GKGGKGLGKGGAKR) in total and BRD4-immunoprecipitated chromatin from

spermatocytes (Sc), round spermatids (RSp) and elongating/condensing spermatids (E/CSp). Standard deviation is calculated for two biological replicates.

	Avg Total	St Dev Total	Avg BRD4 IP	St Dev BRD4 IP
Sc				
Unmodified	48.75%	0.89%	53.01%	18.06%
1ac	39.41%	1.37%	27.42%	2.80%
2ac	10.45%	2.52%	9.88%	8.31%
3ac	0.94%	0.15%	3.60%	2.42%
4ac	0.45%	0.10%	6.09%	4.52%
RSp				
Unmodified	30.39%	0.46%	37.40%	4.57%
1ac	57.27%	1.28%	40.78%	2.51%
2ac	8.67%	1.13%	7.70%	0.49%
3ac	2.26%	0.01%	4.27%	1.52%
4ac	1.42%	0.32%	9.85%	3.08%
E/CSp				
Unmodified	35.91%	0.72%	42.74%	7.08%
1ac	34.90%	3.29%	35.69%	3.77%
2ac	12.51%	0.63%	11.43%	1.50%
3ac	8.55%	0.76%	5.78%	1.22%
4ac	8.12%	1.18%	4.35%	0.59%

FIGURE LEGENDS

Figure 1: BRD4 is expressed in meiotic cells and spermatids, but not in mature sperm

(A) Schematic of the progression of spermatogenesis beginning with meiotic cells (spermatocytes) and progressing through spermiogenesis from round to elongating to condensing spermatids. Changes in cell (tan) and nucleus (blue) size and shape are shown for reference in figures to follow.

(B) Western blot analysis of whole cell extracts from spermatocytes (Sc), round spermatids (RSp), elongating/condensing spermatids (E/CSp), a mixture of round, elongating, and condensing spermatids (R/E/CSp) obtained with STA-PUT velocity sedimentation, and

mature sperm (Sperm). Asterisks mark the full length BRD4 isoform and the arrow indicates a novel shorter BRD4 peptide in spermatids. Peptide competition of BRD4 antibody shows specificity of the BRD4 antibody.

Figure 2: BRD4 forms a ring around the nucleus of spermatids as histones become hyper-acetylated

(A) Indirect immunofluorescence of cryosectioned mouse testes tissue shows that BRD4 (green) forms a ring around the nucleus (DAPI-stained DNA shown in blue) of early (top panel) to late (bottom panel) elongating spermatids. The ring is absent in all non-spermatid cell types such as spermatocytes (Sc).

(B) Indirect immunofluorescence of cryosectioned mouse testes tissue shows that the BRD4 ring (green) forms at the onset of histone H4 hyper-acetylation (red) in the nucleus (DAPI in blue) of early (top panel) to late (bottom panel) elongating spermatids.

Stage of spermatogenesis shown in upper left hand corner of each panel. Separation of spermatocytes (Sc) and spermatids (Sp) within the seminiferous tubule is indicated with a grey dotted line. Inset shows 3x magnification of the spermatids outlined with a dotted square.

(C) and (D) Indirect immunofluorescence of a mixed population of spermatogenic cells shows that BRD2 and BRDT (red) are diffusely localized in the nuclei (DAPI in blue) of spermatocytes (Sc) and round spermatids (RSp), but not condensing spermatids (CSp). Scale bar represents 10μm.

Figure 3: BRD4 forms a ring within the nuclear envelope at the base of the acrosome

(A) Indirect immunofluorescence of BRD4 (green), Lamin B1 (red), and DAPI-stained DNA (blue) in a round spermatid. Asterisk indicates location of the acrosome.

(B) Indirect immunofluorescence of Lamin B1 (green), the acrosome (detected with PNA in red), and DAPI-stained DNA (blue) in a round spermatid.

(C) Indirect immunofluorescence of BRD4 (green), acrosome (detected with PNA in red), and DAPI-stained DNA (blue) in a round spermatid (top), early elongating spermatid (middle), and condensing spermatid (bottom).

(D) Indirect immunofluorescence of fluorophore-conjugated streptavidin (red) with (top) or without (bottom) JQ1-biotin and DAPI-stained DNA (blue) in a mixed population of spermatogenic cells.

(E) Indirect immunofluorescence of BRD4 (green), JQ1-biotin (red), and DAPI-stained DNA (blue) in a late round (top panel) and elongating (bottom panel) spermatid.

(F) Indirect immunofluorescence of the acrosome (detected with PNA in green), JQ1-biotin (red), and DAPI-stained DNA (blue) in a condensing spermatid.

Scale bar represents 5μm (A-C,E,F) and 10μm (D).

Figure 4: BRD4 does not form a ring in *Hrb*$^{-/-}$ acrosomal mutant mice

(A) Indirect immunofluorescence of the acrosome (detected with PNA in green) and DNA (DAPI in blue) in testes tissue sections from wild-type and *Hrb*$^{-/-}$ mice. The stage of spermatogenesis is shown in the upper left hand corner of each panel.

(B) Indirect immunofluorescence of BRD4 (green) and DNA (DAPI in blue) in elongating spermatids of cryosectioned testes tissue from *Hrb*$^{+/-}$ (left) and *Hrb*$^{-/-}$ (right) mice.

Inset shows 3x magnification of the spermatids outlined with a dotted square. Scale bar represents 10μm.

Figure 5: BRD4 is enriched at the promoters of active genes in round spermatids

(A) ChIP sequencing of BRD4 and various histone PTMs reveals that BRD4 and histone H3 and H4 acetylation are associated with gene-rich regions of the genome while H3K9me3 is enriched in intergenic, gene poor regions. UCSC-defined genes are shown at the bottom in dark blue. Genomic location is indicated at the top. The y axis is ChIP enrichment (normalized to input). The x axis is DNA sequence.

(B) Percentage of defined ChIP-seq peaks of BRD4, BRDT, and various histone PTMs in promoter (1kb upstream of the TSS), gene (intron versus exon), or intergenic regions in round spermatids.

(C) ChIP sequencing of BRD4 and various histone PTMs at housekeeping (*Actb*) and spermatogenesis-specific (*Tnp1*) transcriptionally active genes and an inactive gene, *Myc*. BRD4 is not present at all gene promoters that are enriched for H3/H4 acetylation (*Vps45*). UCSC-defined genes are shown at the bottom in dark blue. The y axis is ChIP enrichment (normalized to input). The x axis is DNA sequence.

Figure 6: BRD4 and BRDT bind to different subsets of transcriptionally active genes in round spermatids

(A) Heat map representation of ChIP-sequencing enrichment at promoters of all genes (green) compared to the level of transcription of these genes (red) in round spermatids. Brightness indicates higher levels of enrichment or transcription.

(B) Box and whisker plot of transcription levels of genes that are bound by BRD4, BRDT, or both. Overall transcription levels are shown for spermatogenesis-specific genes ("Sperm.") and all genes, as a reference.

(C) Box and whisker plot of enrichment levels of different histone PTMs at the gene promoters (1kb upstream of the TSS) bound by BRD4, BRDT, or both (presence or absence of binding indicated with "+" or "–", respectively, at bottom).

(D) Pie chart representations of GO Terms of genes enriched for BRD4 (left), BRDT (middle), or both (right) in round spermatids.

(E) ChIP sequencing of BRD4, BRDT, and various histone PTMs at promoters of genes present in the top-most represented GO Term category from the corresponding pie chart in (D) above. UCSC-defined genes are shown at the bottom in blue. The y axis is ChIP enrichment (normalized to input). The x axis is DNA sequence.

(F) Heat map representation of BRD4 and BRDT enrichment around the TSS (± 2.5kb) of spermatogenesis-specific genes in round spermatids. Brightness indicates higher levels of enrichment.

Figure 7: BRD4 association with poly-acetylated histone H4 diminishes in late spermatids as acetylated histones are removed from the condensing nucleus

(A) Mass spectrometry analysis of BRD4-immunoprecipitated histones from round spermatids. Heatmap representation of enrichment of acetylation or methylation of histone H3 (amino acids 9 to 17, KSTGGKAPR) or H4 peptide (amino acids 4 to 17, GKGGKGLGKGGAKR) in BRD4-immunoprecipitated chromatin normalized to total

chromatin (log transformed). Raw values used to generate the heatmaps are found in Table 3.

(B) Comparison of degree of H4 peptide acetylation (amino acids 4 to 17, GKGGKGLGKGGAKR) in total and BRD4-immunoprecipitated (IP) chromatin over the course of spermatogenesis. Black and grey bars indicate changes in H4 acetylation from spermatocytes (Sc) to round spermatids (RSp) and from round spermatids to elongating/condensing spermatids (ECSp), respectively, via log-transformed ratio of percentage acetylated H4 peptide. Raw values used to generate the graphs are found in Table 4.

(C) Indirect immunofluorescence of BRD4 (green), H4K5,8,12,16ac (red), and DAPI-stained DNA (blue) in a condensing spermatid. Scale bar represents 5μm.

(D) Model showing the locations of different cellular features associated with the spermatid nucleus. BRD4 (green) forms a ring structure between the nucleus (blue) and the acroplaxome (red) in a key region of the nuclear membrane where the Lamin B1- and nuclear pore-enriched posterior portion meets the acrosome-associated, nuclear pore-depleted anterior portion.

Bryant_Fig1

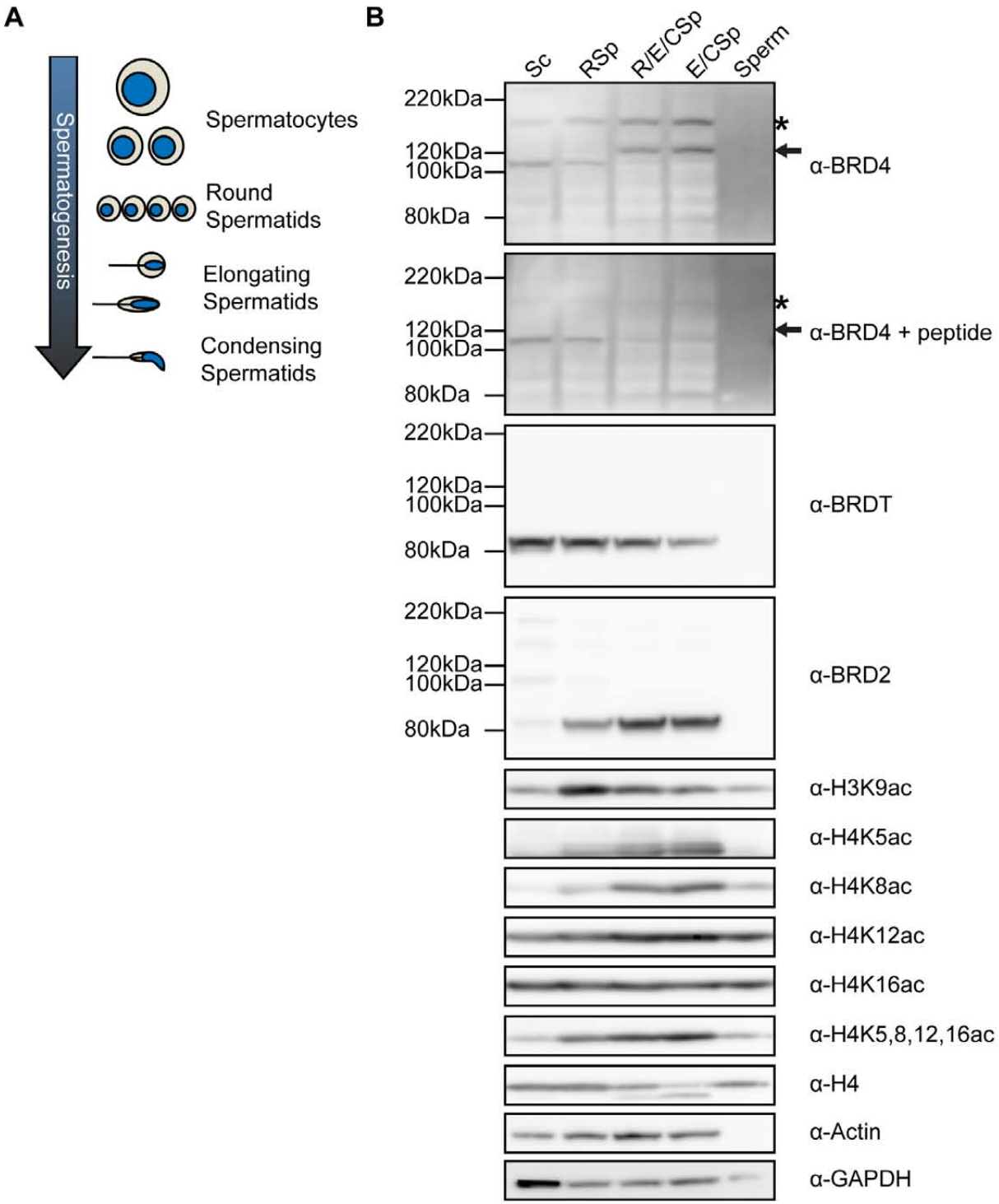

Bryant_Fig2

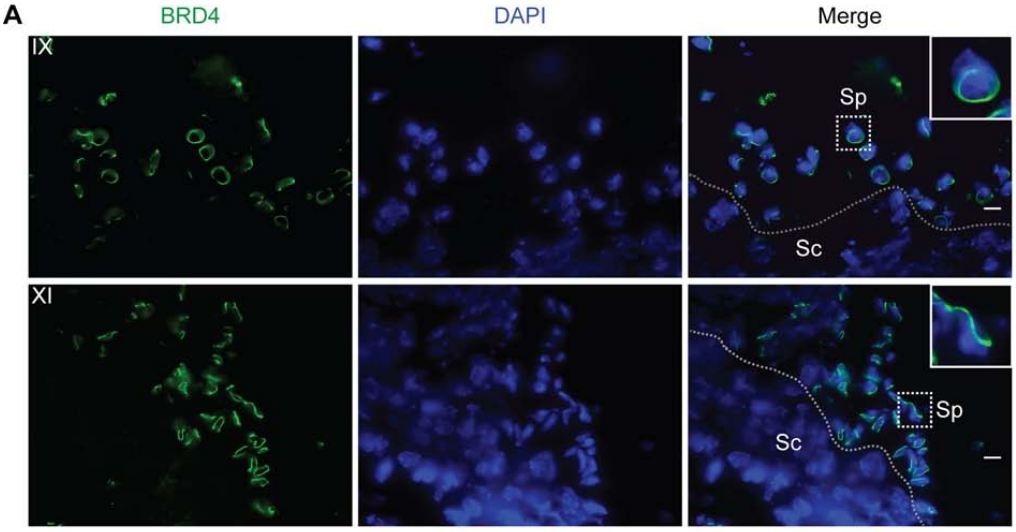

Bryant_Fig2

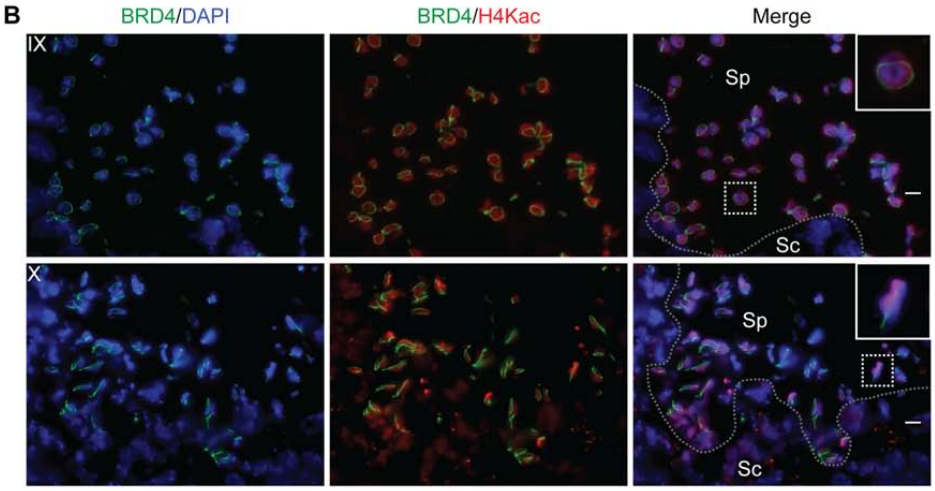

Bryant_Fig2

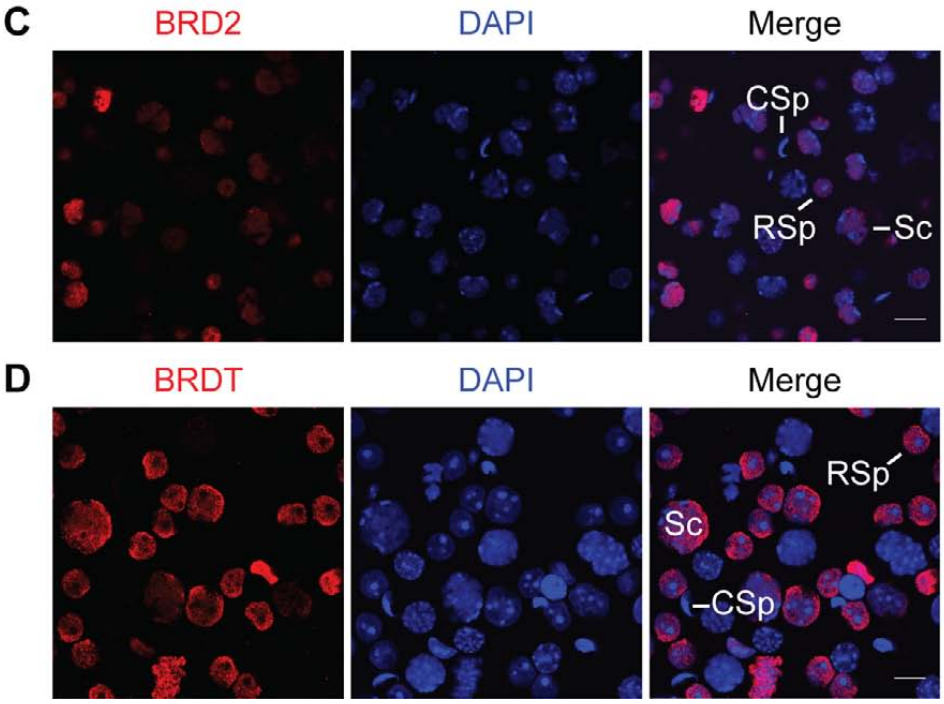

Bryant_Fig3

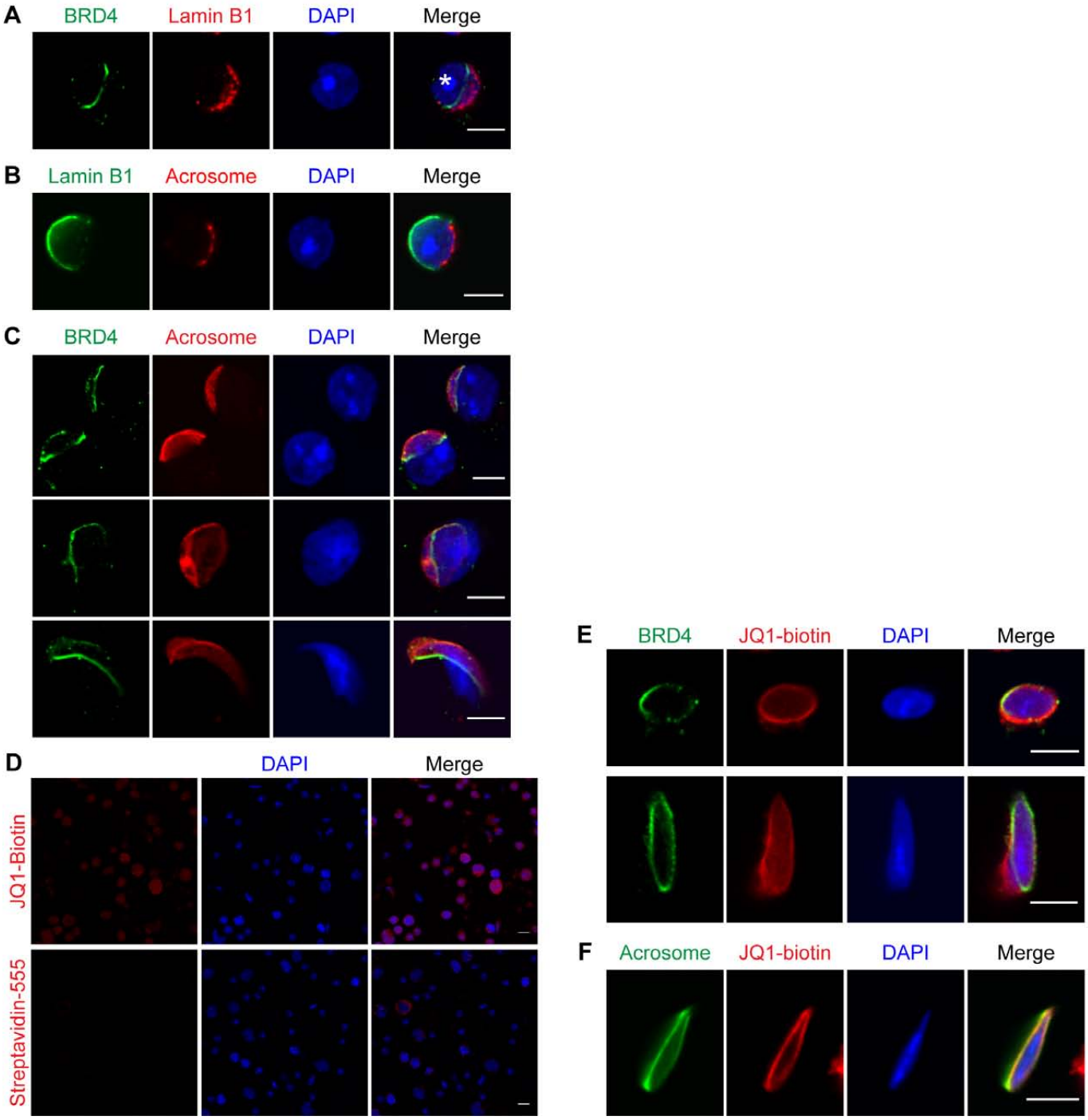

Bryant_Fig4

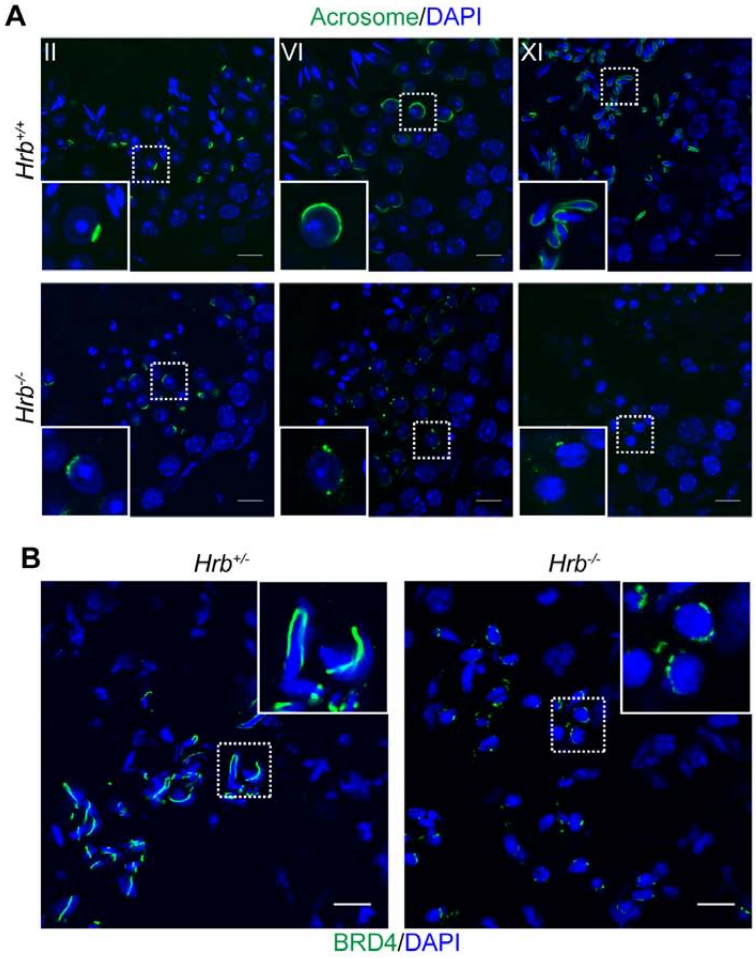

Molecular and Cellular Biology

Bryant_Fig5

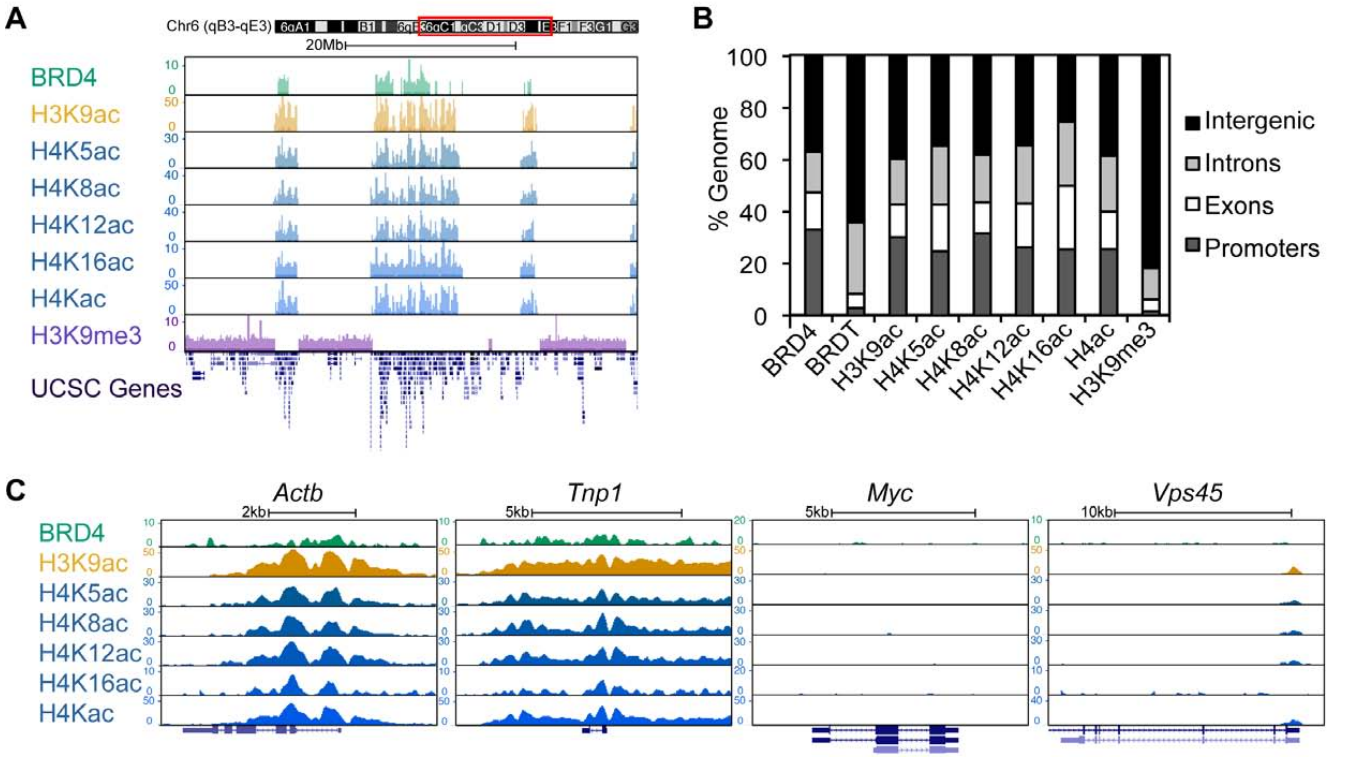

Bryant_Fig6

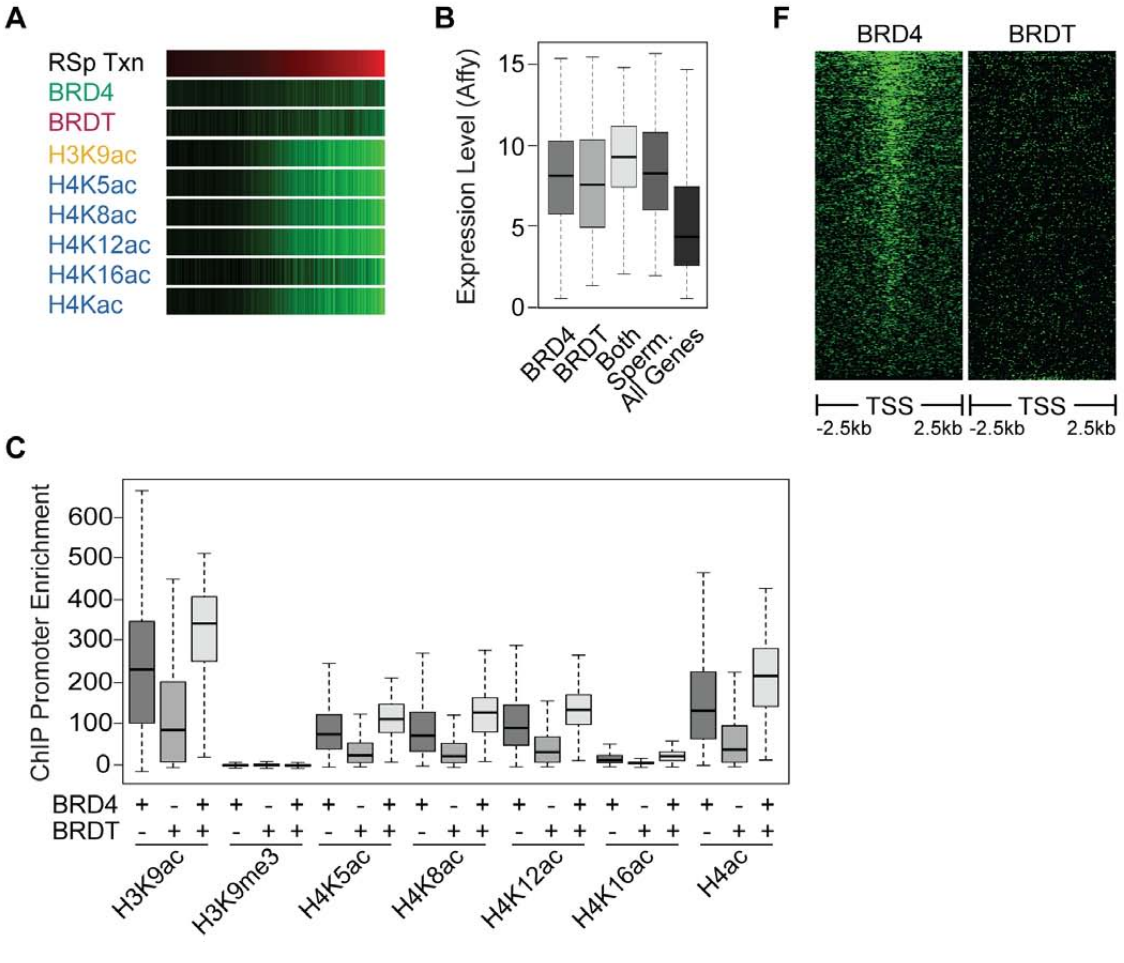

Bryant_Fig6

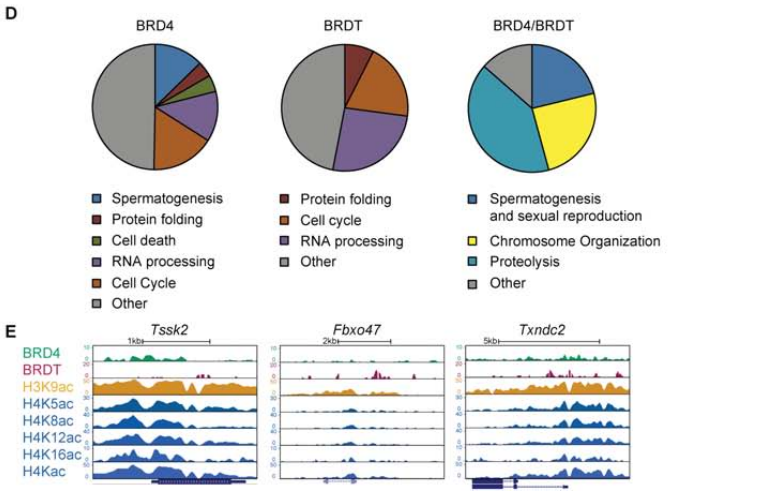

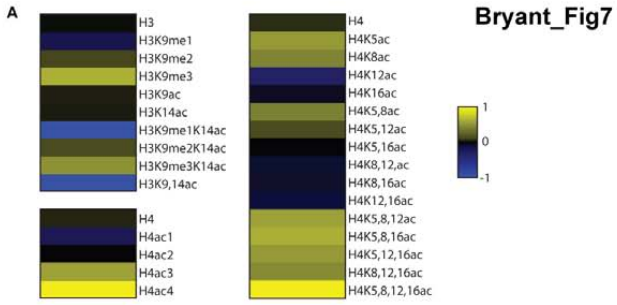

Bryant_Fig7